Prepared for submission to JINST

Design and test for the CEPC muon subdetector based on extruded scintillator and SiPM

Hongyu Zhang,[a] Xiyang Wang,[a] Weihu Ma,[a] Shiming Zou,[a] Deqing Fang,[a] Wanbing He,[a,b] Xiaolong Wang,[a] Zhen Wang,[c,d,e] Rui Yuan[c,d,e] and Qibin Zheng[f]

[a] *Key Laboratory of Nuclear Physics and Ion-beam Application (MOE) and Institute of Modern Physics, Fudan University,*
220 Handan Road, Shanghai, 200433, China
[b] *Shanghai Research Center for Theoretical Nuclear Physics, NSFC and Fudan University,*
2005, Songhu Rodad, Shanghai, 200438, China
[c] *Tsung-Tao Lee Institute, Shanghai Jiao Tong University,*
520 Shengrong Road, Shanghai 201210, China
[d] *Institute of Nuclear and Particle Physics, School of Physics and Astronomy,*
800 Dongchuan Road, Shanghai 200240, China
[e] *Key Laboratory for Particle Astrophysics and Cosmology (MOE), Shanghai Key Laboratory for Particle Physics and Cosmology (SKLPPC), Shanghai Jiao Tong University,*
800 Dongchuan Road, Shanghai 200240, China
[f] *Laboratory of Radiation Detection and Medical Imaging and School of Health Science and Engineering, University of Shanghai for Science and Technology,*
516 Jungong Rodad, Shanghai, 200093, China

E-mail: xiaolong@fudan.edu.cn

Abstract: The integration of a scintillator, wavelength-shifting fiber, and silicon photomultiplier (SiPM) has demonstrated superior performance in the K-long and Muon detector (KLM) of the Belle II experiment. This study outlines our research and development (R&D) initiatives aimed at harnessing similar detection technologies, incorporating a novel scintillator and SiPM, for potential use in a muon detector for the proposed Circular Electron Positron Collider (CEPC) experiment. Our R&D activities have been focused on evaluating the efficacy of a newly developed 150 cm-long scintillator, alongside the NDL SiPM featuring a sensitive area of 3 mm $\times$ 3 mm, or the Hamamatsu MPPC with a 1.3 mm $\times$ 1.3 mm sensitive surface. The project also includes the fabrication of a detector strip and the implementation of techniques designed to optimize light collection efficiency. Cosmic ray testing has shown that both NDL SiPMs and MPPCs are capable of highly efficient photon collection, achieving efficiencies significantly exceeding 90% when employing a threshold of 8 photoelectrons. Additionally, the time resolution for detecting events at the distal end of a scintillator strip has been measured to be better than 1.7 ns. The remarkable performance observed suggests that this technology holds great promise as a highly effective muon detector for the CEPC.

Keywords: Muon spectrometers; Scintillators and scintillating fibres and light guides; Photon detectors for UV, visible and IR photons (solid-state) (PIN diodes, APDs, Si-PMTs, G-APDs, CCDs, EBCCDs, EMCCDs, CMOS imagers, etc); Performance of High Energy Physics Detectors

ArXiv ePrint: 2312.02553

[1]Corresponding author.

Contents

1 Introduction **1**

2 Belle II KLM and scheme of a detector channel **2**

3 The major components for a detector channel **3**

3.1 Scintillator and WLS fiber 3

3.2 Hamamatsu MPPCs and NDL SiPMs 4

3.3 Readout electronics and data acquisition system 5

4 Improvements for the photon collection **6**

5 Performance of an array of scintillator strips in cosmic ray tests **7**

6 summary **8**

1 Introduction

In the framework of the Standard Model of particle physics, the Higgs boson (H) is pivotal in shedding light on the origin of mass for matter. With the Higgs boson's mass approximately $m_H \approx 125$ GeV/c^2, it enables the conceptualization of a new e^+e^- collider. This collider would operate at a center-of-mass energy of $\sqrt{s} \sim 240$ GeV, effectively serving as a Higgs factory. Several initiatives, including the International Linear Collider [1, 2], the Circular Electron Positron Collider (CEPC) [3, 4], and the Future Circular Collider [5], have been proposed in pursuit of this goal. The CEPC proposal, initiated in 2013, has since been followed by extensive research and development (R&D) efforts focused on both the accelerator and the detector components.

The primary process for Higgs boson generation via e^+e^- annihilation is $e^+e^- \rightarrow H + Z^0$, allowing for the precise determination of the H boson through the recoil of the Z^0 boson, which exhibits a branching fraction of $(3.3662 \pm 0.0066)\%$ for decay into a $\mu^+\mu^-$ pair [6]. Consequently, the muon detector is of paramount importance in a Higgs factory setting. Beyond the reconstruction of $Z^0 \rightarrow \mu^+\mu^-$, the presence of muons in the final state is often regarded as the "golden channel" in new particle searches [7]. As outlined in the Conceptual Design Report for the CEPC, its muon detector is tasked with muon identification, calibrating shower leakage from calorimeters, and probing for long-lived particles [4]. The muon detection system is expected to excel in detection efficiency, maintain a low rate of hadron misidentification, ensure precise position resolution, and achieve broad coverage. Additionally, clear muon signals are invaluable for enhancing the trigger system's performance. The proposed layout for the CEPC muon detector, consisting of a barrel and two endcaps, incorporates eight sensitive layers interposed with iron absorbers. This configuration is designed to achieve high standalone muon detection efficiency (95%), requiring minimum position

resolutions $\sigma_{r\phi} = 2.0$ cm, $\sigma_z = 1.5$ cm, alongside precise time resolution and a rate capability ranging from 50 – 100 Hz/cm^2, thereby facilitating crucial muon momentum insights [4].

In this article, we detail the R&D efforts for the CEPC muon detector, employing scintillator-based technology akin to the KLM of the Belle II experiment [8]. During the initial Belle experiment, Resistive Plate Chambers (RPCs) were utilized within the KLM [9]. However, the prolonged recovery time of RPCs, when operating under high luminosity conditions, led to a noticeable drop in efficiency, prompting the partial substitution with scintillator modules. These modules, composed of plastic scintillator strips, wavelength-shifting (WLS) fibers, and silicon photomultipliers (SiPMs), have demonstrated effective performance in Belle II [10]. Their operation not only meets but also largely aligns with the stringent requirements set for a muon detector in the CEPC, showcasing their potential for future applications.

2 Belle II KLM and scheme of a detector channel

As the outermost component of the Belle II detector, the KLM system plays a crucial role in identifying K_L mesons and muons, capable of detecting particles with momenta up to 4.5 GeV/c. The KLM extends over radii from 200 to 240 cm in its octagonal barrel section and from 130 to 340 cm in the forward and backward endcaps, as illustrated in Fig. 1(a). The barrel configuration includes 15 layers of detector elements interleaved with 14 layers of yoke iron, whereas each endcap is structured with 14 detector and 14 iron layers. These yoke layers fulfill a dual purpose: facilitating magnetic flux return for the solenoid and aiding in the clustering of hadron cascades for K_L detection. Detector panels, approximately 3.1 cm in thickness, are strategically placed within the gaps of steel plates, each 4.7 cm thick, to enhance particle detection efficiency. The detector's architecture incorporates scintillator strips within the two innermost layers of the barrel and throughout all layers of the endcaps, whereas the remaining 13 barrel layers utilize the legacy RPCs from the original Belle experiment. This design allows for precise two-dimensional localization of particle trajectories through orthogonal hits on the scintillator strips. The KLM boasts around 38,000 readout channels, half of which are dedicated to the scintillator-based detections, showcasing the system's extensive coverage and high-resolution particle tracking capabilities.

In the design of scintillator modules for the Belle II KLM detector, the cross-sectional dimensions of the scintillator strips are tailored for their specific locations: 4 cm $\times$ 1 cm for the barrel and 4 cm $\times$ 0.75 cm for the endcaps, achieving a spatial resolution of approximately $\sigma_s \approx 1.2$ cm. Each strip incorporates a Kuraray Y11(200)MSJ WLS fiber [11] to efficiently capture and guide photons towards a SiPM, also known as a Multi-Pixel Photon Counter (MPPC: Hamamatsu S10362-13-050C), which is directly attached to one end of the WLS fiber. The MPPC enhances the initial signal by an internal preamplification factor of about 10, after which the signals are transmitted through ribbon cables to the external readout electronics located on the magnet yoke. Figure 1(b) illustrates the interior of a scintillator module developed at Virginia Tech for the barrel section of KLM in 2013. Further details on the development and testing of the scintillator modules for the Belle II endcap KLM are provided in Ref. [12].

We adopted a design inspired by the Belle II KLM for our detector channel, utilizing an extruded scintillator as depicted in Fig. 2. This detector channel comprises a lengthy scintillator strip, measuring 1 cm $\times$ 4 cm $\times$ 150 cm, which houses a WLS fiber. A SiPM is mounted on

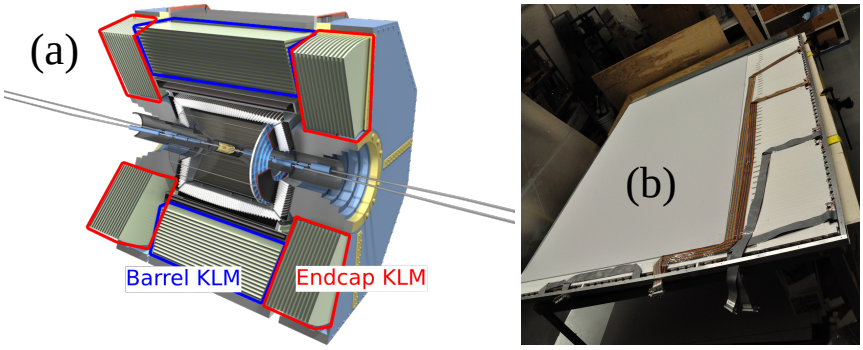

Figure 1. The KLM system in the Belle II detector and a scintillator module for the barrel KLM.

a compact printed circuit board (PCB) and connected to the WLS fiber via a custom-designed coupling component, ensuring efficient signal transfer.

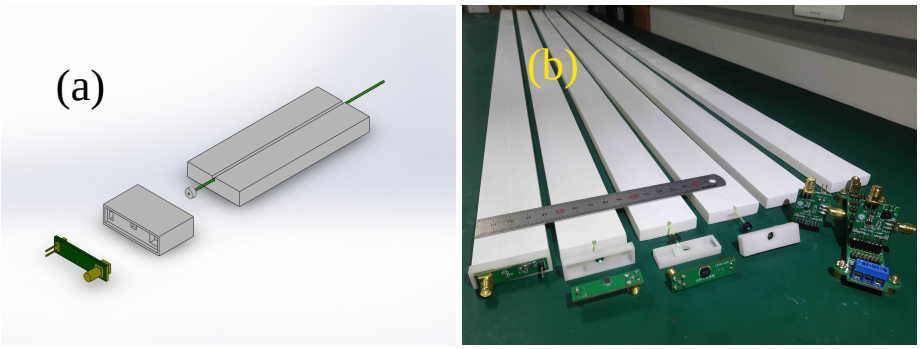

Figure 2. The architecture of a detector channel includes an elongated scintillator strip, measuring 150 cm × 4 cm × 1 cm, equipped with an internal WLS fiber. A SiPM is positioned on a compact PCB featuring a preamplifier. Additionally, the design incorporates connectors for securing the fiber and facilitating its connection to the SiPM.

3 The major components for a detector channel

A detector channel comprises four key elements: a scintillator strip, a WLS fiber, a SiPM, and an front-end electronic readout equipped with a preamplifier. The readout design [13] was meticulously crafted, while the scintillator strips and SiPMs were custom-produced by manufacturers in Beijing. Additionally, we procured the identical WLS fiber utilized in the Belle II KLM experiment directly from Kuraray.

3.1 Scintillator and WLS fiber

Efficiencies exceeding 90% have been achieved at the distal end with scintillator strips from renowned producers such as Fermilab and Uniplast for the Belle II KLM [8]. In this R&D work, the scintillator strips are produced by GaoNengKeDi company [14] using a polyethylene extrusion

technique [15]. The inherent short attenuation length of such scintillators, only several centimeters, poses challenges in long detector strips, whereas a WLS fiber boasts an attenuation length of several meters. To accommodate the WLS fiber, a long groove, approximately 2 mm wide and 4 mm deep, is embedded within the scintillator. We evaluated both the BCF-92 fiber from Saint-Gobain [16, 17] and the Y11(200) fiber from Kuraray [11], with diameters of 1.0 mm and 1.2 mm, respectively. Light yield performance of the two WLS fibers was assessed by comparing the activated pixels of the SiPM. The tests indicate that the light yield with Kuraray fiber is typically 2.3 times higher than that with Saint-Gobain fiber.

The Y11(200) fiber acts as a blue-to-green wavelength shifter with an emission spectrum peaking at 476 nm [11]. According to its datasheet, Y11(200) fiber has an attenuation length exceeding 3.5 m. Light yields of the scintillator coupled with Y11(200) fiber were measured at various positions in cosmic ray tests and modeled with two exponential decay functions. The effective attenuation lengths derived from these functions are (2.63 ± 0.37) m and (5.8 ± 1.1) cm, respectively.

3.2 Hamamatsu MPPCs and NDL SiPMs

A SiPM consists of a densely packed array of avalanche photodiodes, each operating in Geiger mode. This technology is celebrated for its exceptional photon detection efficiency, substantial gain, superior time resolution, low operational voltage, durability, and immunity to magnetic fields. The quantum efficiency of a SiPM typically approaches 50%. Upon photon arrival, the SiPM's pixels trigger through the photoelectric effect, generating and amplifying electrons. This includes the generation of thermally induced electrons in the absence of photon input, known as dark counting. An electron thus generated and amplified in a SiPM, whether from an actual signal or dark counting, is termed a photo-electron ($p.e.$). The output pulse amplitude is directly proportional to the number of photoelectrons ($N_{p.e.}$), distinguishable in the SiPM's Analog-to-Digital Converter (ADC) signal distribution.

In our research, we utilize two variants of SiPMs: the S13360 series MPPC with a pixel size of 50 µm, produced by Hamamatsu, and the EQR15 11-3030D-S series SiPM with a 15 µm pixel size, developed by the Novel Device Laboratory (NDL). The S13360 series MPPCs, in comparison to the S10362 series used in the existing KLM detector of Belle II, offer an identical sensitive area of 1.3 mm $\times$ 1.3 mm, but with lower operational voltages and decreased rates of cross-talk and dark counting (DCR). The EQR15 11-3030D-S series presents a larger sensitive area of 3.0 mm$\times$3.0 mm, significantly surpassing the cross-section of the Y11(200) WLS fiber.

Prior to their integration into our setup, we thoroughly investigate the Hamamatsu MPPCs and NDL SiPMs for key characteristics: breakdown voltage, gain, DCR, and cross-talk. Breakdown voltage refers to the reverse bias voltage at which the SiPM begins functioning via avalanche amplification. The gain of a SiPM quantifies the charge it accumulates from a single $p.e.$ signal (SPE). Experimental evaluations demonstrate gains of 1.1×10^5 for the S13360 MPPC at an operational voltage of 57.0 V, and 0.7×10^5 for the EQR15 11-3030D-S at 27 V.

Dark counting in SiPMs presents a challenge for photon detection, particularly for SPE detection. The DCR of an SiPM is determined by counting the number of dark pulses surpassing a specified $N_{p.e.}$ threshold. In this context, we set the threshold at 0.5 $p.e.$. Optical cross-talk is assessed by comparing the DCR for pulses exceeding thresholds of 1.5 $p.e.$ and 0.5 $p.e.$. As

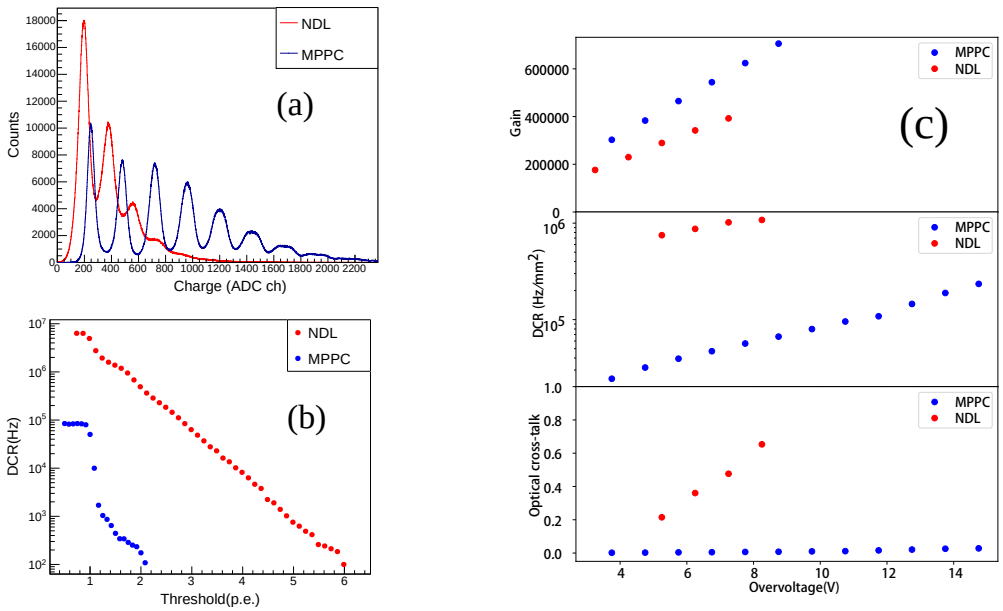

Figure 3. Characteristics of the SiPMs employed in the R&D for the CEPC Muon Detector. Plot (a) illustrates the photon detection spectra for the Hamamatsu MPPC at a bias of 56.0 V and the NDL SiPM at 27.0 V. In these spectra, up to 8 $p.e.$ peaks are discernible for the MPPC, whereas for the NDL SiPM, peaks up to 4 $p.e.$ are observable. Plot (b) delineates the DCR for both MPPC and NDL SiPM as a function of the $N_{p.e.}$ threshold. Lastly, plot (c) presents the relationship between the overvoltage and the corresponding variations in gain, DCR, and optical cross-talk for both MPPC and NDL SiPM devices.

illustrated in Fig. 3, NDL SiPMs exhibit significantly higher DCR and greater optical cross-talk compared to Hamamatsu MPPCs, a discrepancy attributed in part to their smaller pixel size.

3.3 Readout electronics and data acquisition system

SiPM operation generally necessitates a signal amplification circuit and an external power supply. We have developed a new preamplifier that achieves a time resolution superior to 50 ps and a gain of 21 [13]. To enhance gain stability, we implemented negative feedback in its design. Additionally, we engineered a power supply motherboard equipped with a voltage regulator module. This module provides both high voltage for SiPM functioning and low voltage for the preamplifier operations.

For signal waveform data collection, we employed a Tektronix MSO58 oscilloscope, which was PC-controlled and equipped with trigger logic [18]. This setup allowed us to efficiently store waveform data. The data acquisition system operated at a bandwidth of 20 MHz, with a sampling rate of 3.125 GS/s, and captured data within a 400 ns window. Through offline analysis of these waveforms, we extracted comprehensive data on ADC, TDC, baseline stability, timing accuracy, and more. Specifically, we examined pulse heights or ADC counts to estimate the $N_{p.e.}$ and utilized the leading edge or constant fraction discrimination method to derive precise timing information.

4 Improvements for the photon collection

The coupling between the fiber, scintillator, and SiPM is crucial for the detector channel's performance, impacting detection efficiency and time resolution. We developed a coupling component to secure the WLS fiber and SiPM together, polished the end of the WLS fiber, applied a reflective coating to the scintillator, and filled the scintillator groove with optical glue. To evaluate performance, we triggered cosmic rays passing through the long strip at various positions using two short strips positioned above and below. The $N_{p.e.}$ distribution from the SiPM signals was fitted with a Landau function. The plotted points and their error bars in Fig. 4 represent the fitted results, indicating the number of activated pixels. Here, the y-axis value and the error bar of each point represent the mean and the standard deviation (σ) of the Landau function.

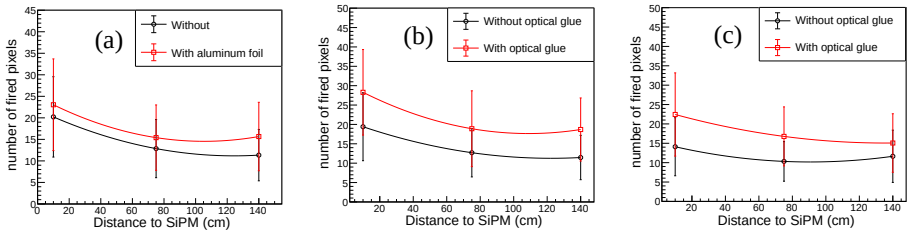

Figure 4. The distribution of the average $N_{p.e.}$ varies according to the distance between the impact point on the scintillator strip and the SiPM. Plot (a) compares the scenarios with and without aluminum foil. Plots (b) and (c) showcase the effects of using optical glue with TiO_2 and Teflon, respectively. The data points and their error bars represent the mean values and standard deviations derived from fitting the $N_{p.e.}$ distributions with Landau functions.

The coupling mechanism used in the Belle II experiment has been enhanced in our R&D to streamline the assembly of the detection system and enhance photon detection efficiency. As illustrated in Fig. 2, this modified component ensures a robust connection between the WLS fiber's end and the SiPM's sensitive area. These components are fabricated using a 3D printer for precision and consistency.

The fiber's end is polished with sandpaper, and we find that a 2000 mesh provides a sufficiently smooth surface. This refinement is particularly beneficial for employing the MPPC S13360, which has a sensitive area of 1.3 mm $\times$ 1.3 mm. In the Belle II experiment, the proximity between the fiber and the SiPM was found to influence photon collection by approximately 37%, primarily due to diffuse transmission at the fiber's end. The NDL EQR15 11-3030D-S, featuring a much larger sensitive area of 3.0 mm $\times$ 3.0 mm, demonstrates that meticulous polishing of the fiber's end is not critical for enhancing photon collection with this model.

Reflective coatings such as TiO_2 and Teflon are applied to the scintillator strips to enhance light reflection. Additionally, aluminum foil and black plastic tapes are used to isolate the strips from ambient light and minimize cross-talk. Our comparisons indicate that aluminum foil not only shields against external light interference but also augments light collection, boosting $N_{p.e.}$ by 38% at the strip's far end, as depicted in Fig. 4(a). Tests comparing reflective coatings showed that TiO_2 slightly outperforms Teflon, as presented in Figs. 4(b) and 4(c). However, Teflon offers production

simplicity and cost-effectiveness, suggesting that a thicker Teflon layer could be advantageous for further optimization.

We use optical glue to enhance the coupling between the fiber and the scintillator. In a test involving TiO_2-coated strips, the application of optical glue yields a substantial increase of 63% in $N_{p.e.}$ at the far end of the strips, as shown in Fig. 4(b). Additionally, Teflon-coated strips exhibited a 30% improvement, as shown in Fig. 4(c).

Optical glue is utilized to strengthen the bond between the fiber and the scintillator. In tests with TiO_2-coated strips, using optical glue resulted in a significant 63% increase in $N_{p.e.}$ at the strip's far end, illustrated in Fig. 4(b). Similarly, Teflon-coated strips showed a 30% improvement, as seen in Fig. 4(c), underscoring the efficacy of optical glue in enhancing photon collection efficiency.

5 Performance of an array of scintillator strips in cosmic ray tests

Similar to the KLM in the Belle II experiment as depicted in Fig. 1, a muon detector usually comprises multiple layers of detector modules for effective charged track identification. Drawing from our experience with the KLM, the cornerstone of muon detector R&D, particularly when utilizing extruded scintillators, is achieving high efficiency across all scintillator strips. To evaluate collective performance, we assembled an array of six detector channels and conducted cosmic ray tests, as illustrated in Fig. 5(a). For triggering, we positioned two short strips, each 10 cm in length, vertically at both ends of the six longer strips. The optimal operating voltages determined for the MPPC S13360 and NDL EQR15 11-3030D-S SiPMs are 56 V and 27 V respectively, based on their performance metrics presented in Fig. 3. The signal amplitudes for SPE events from these SiPMs approximate 2 mV. Figure 5(b) displays typical signal waveforms captured from the two trigger strips and the six detector strips.

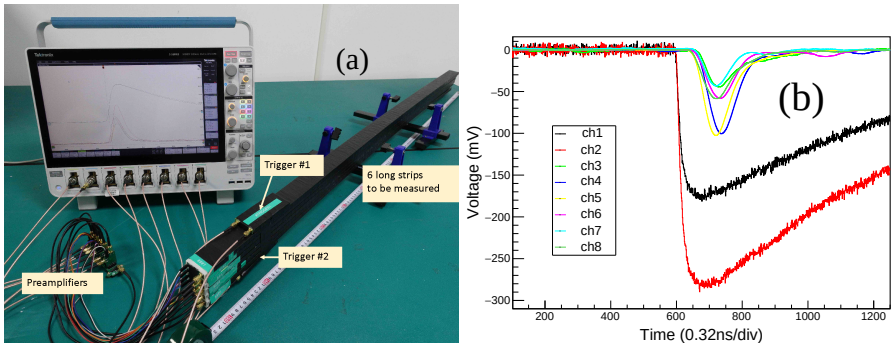

Figure 5. Setup for the cosmic ray test of six long strips, incorporating preamplifiers and an oscilloscope, alongside the oscilloscope-captured waveforms of six channels and two trigger channels at the distal end. In plot (b), ch1 and ch2 correspond to Trigger#1 and Trigger#2, as depicted in plot (a), with ch3-ch8 representing the six long strips. The pulse profiles for both NDL and MPPC display resemblance.

Similar to the approach detailed in Fig. 4, we evaluated the ADC distributions of the array at various positions and then converted these into distributions of $N_{p.e.}$. We employed Landau functions for fitting the $N_{p.e.}$ distributions and presented the resultant means and standard deviations in Figs. 6(a1) and 6(a2). The array, equipped with NDL SiPMs, exhibited consistent photon

collection performance, achieving up to 34 $p.e.$s per cosmic ray event at the proximal end and 23 $p.e.$s at the distal end, with the use of aluminum foil enhancing the reflective layer. Despite the variance in cross-talk levels, both NDL SiPMs and Hamamatsu MPPCs showed comparable photon collection efficiencies. The absence of a significant decline in $N_{p.e.}$ beyond a 75 cm distance underscores the advantage of the WLS fiber's extended attenuation length for maintaining high detection efficiency along the length of the scintillator strip.

As shown in Figs. 6(b1) and 6(b2), efficiency assessments at the distal end for the six strips, fitted with either MPPCs or NDL SiPMs, revealed that most strips equipped with NDL SiPMs maintained efficiencies above 90% at a threshold of 10.5 $p.e.$s. Strips with MPPCs also demonstrated high efficiency, exceeding 84% at the same threshold. These findings underscore the effectiveness of both NDL and MPPC SiPMs in capturing events at the farther reaches of the strips. It is important to note that some variance among the six strips can be attributed to the assembly quality of the SiPM and fiber.

Based on the results at operational voltages, the optical cross-talk for NDL EQR15 11-3030D-S SiPMs is around 20%, while it is about 1% for MPPC S13360. Performance evaluation using strip response thresholds shows that 90% of cosmic rays trigger a response in all MPPC strips, compared to 70% with NDL SiPMs. Achieving a cosmic ray detection efficiency of approximately 95% with NDL SiPMs and 99% with MPPCs indicates that the high-efficiency design criteria for CEPC are satisfied. This suggests the potential for a highly efficient, robust, and compact muon detector using scintillators, WLS fibers, and SiPMs.

A key advantage of a scintillator-based muon detector is its superior time resolution. The time resolution of KLM built with RPCs was not considered in Belle. With the time calibration, which started from the Belle II Fudan group, the time resolution of Belle II KLM achieves about 4 ns in endcaps and 8 ns in the barrel, with ongoing work for further enhancements. Our study on detector channel time resolution used cosmic rays, employing a trigger system with long attenuation scintillator strips and four large SiPMs per strip, yielding about 60 ps time resolution. By positioning triggers along the strip and measuring time differences, we calculated the strip's time resolutions. Results from MPPC S13360 and NDL EQR15 11-3030D-S tests are shown in Figs. 6(c1) and 6(c2), demonstrating that time resolution at a strip's distal end strongly correlates with the $N_{p.e.}$. Achieving a time resolution under 1 ns requires $N_{p.e.} > 35$ for NDL SiPMs and $N_{p.e.} > 30$ for MPPCs, suggesting that enhancing the scintillator's light yield or using multiple fibers and large SiPMs can improve time resolution.

Figures 6(d1) and 6(d2) illustrate the time resolutions across different positions on the long strips, with NDL SiPMs showing approximately 1.4 ns and MPPCs about 1.2 ns. A linear fit to the time differences between signals from the long strip detector and the trigger, at various trigger positions, determined the scintillation photon propagation speed in Kuraray fiber as (16.3 ± 2.8) cm/ns.

6 summary

For the CEPC muon detector's design, research on using extruded plastic scintillator, WLS fiber, and SiPM is conducted. The GNKD company's scintillators, Hamamatsu and NDL's SiPMs, and Kuraray's WLS fiber are used. SiPM performance enhancement and photon collection improvement

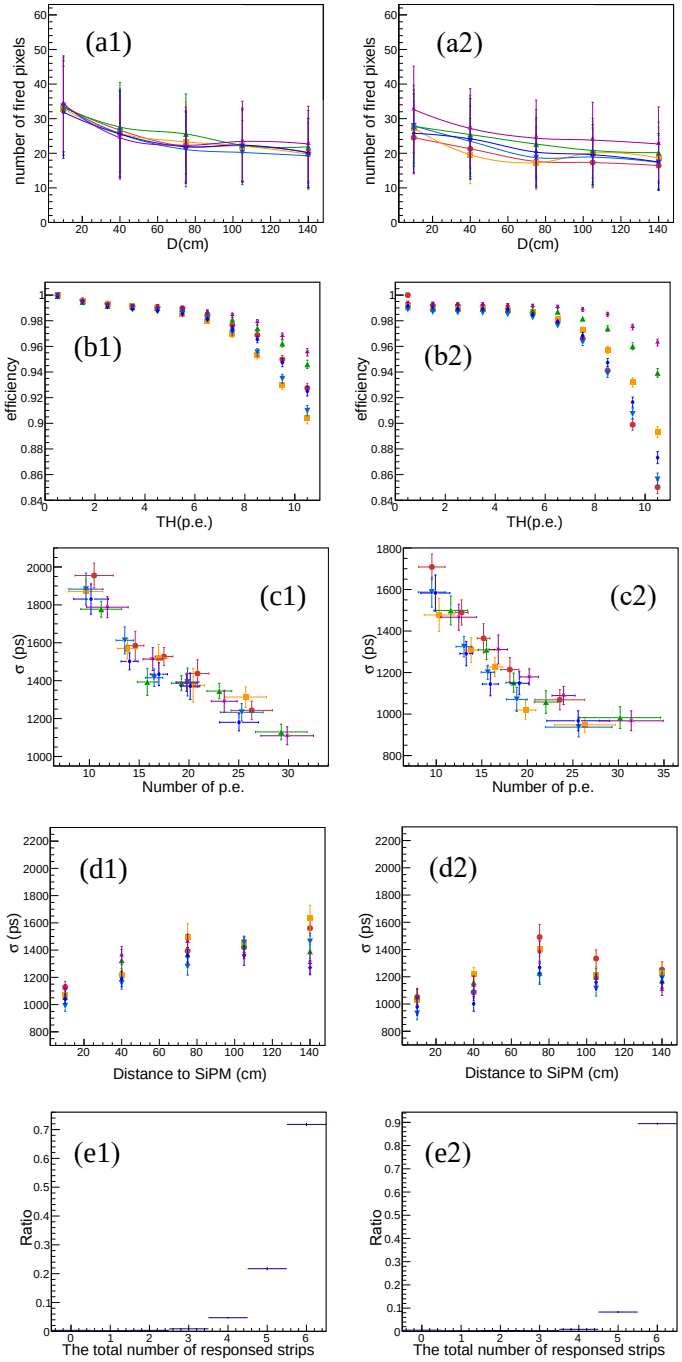

Figure 6. The performance of the detector arrays in cosmic ray tests is detailed, showcasing setups based on NDL SiPMs and Hamamatsu MPPCs, each with six detector channels. Plots (a1) and (a2) are the distributions of $N_{p.e.}$ from the cosmic ray hits along the strips, where the dots and the error bars are the means and the standard deviations from fitting to the $N_{p.e.}$ distributions with Landau functions. Plots (b1) and (b2) are the efficiency versus the $N_{p.e.}$ threshold at the far end. Plots (c1) and (c2) are the time resolutions versus the $N_{p.e.}$ at far end. Plots (d1) and (d2) are the time resolutions triggering at the far ends of the strips. Plots (e1) and (e2) are the distributions of the number of detector channels responding to cosmic ray tracks.

are achieved through a coupling component for WLS fiber and SiPM attachment. Teflon is found to be effective as a reflection layer. The long scintillator strips demonstrate over 90% efficiency and better than 1.7 ns time resolution, indicating the technology's suitability for CEPC's muon detector construction.

Acknowledgments

This work is partially supported by the National Key R&D Program of China under Contract No. 2022YFA1601903; National Natural Science Foundation of China under Contracts No. 11925502, No. 11961141003, and No. 12175041; and the Strategic Priority Research Program of the CAS under Contract No. XDB34030000.

References

[1] C. Adolphsen, M. Barone, B. Barish *et al.*, The International Linear Collider Technical Design Report - Volume 3.II: Accelerator Baseline Design, arXiv:1306.6328. doi:10.48550/arXiv.1306.6328

[2] T. Behnke, J. E. Brau, P. N. Burrows *et al.*, The International Linear Collider Technical Design Report - Volume 4: Detectors, arXiv:1306.6329. doi:10.48550/arXiv.1306.6329

[3] The CEPC Study Group, CEPC Conceptual Design Report: Volume 1 - Accelerator. arXiv:1809.00285v1. doi:10.48550/arXiv.1809.00285.

[4] The CEPC Study Group, CEPC Conceptual Design Report: Volume 2 - Physics & Detector. arXiv:1811.10545v1. doi:10.48550/arXiv.1809.00285.

[5] The FCC Collabration, FCC Physics Opportunities. Eur. Phys. J. C **79** (2019) 474. doi:10.1140/epjc/s10052-019-6904-3

[6] R. L. Workman *et al.* (Particle Data Group), The Review of Particle Physics (2023), Prog. Theor. Exp. Phys. **2022** (2022) 083C01 and 2023 update. doi:10.1093/ptep/ptac097

[7] T. Hebbeker, K. Hoepfner, (2020). Muon Spectrometers. Handbook of Particle Detection and Imaging. doi:10.1007/978-3-319-47999-6_19-2

[8] T. Abe, I. Adachi, K. Adamczyk *et al.*, The Belle II Technical Design Report, KEK Report 2010-1, 2010, arXiv:1011.0352v1. doi:10.48550/arXiv.1011.0352.

[9] A. Abashian, K. Gotow, N. Morgan *et al.* (Belle Collaboration), The Belle detector. Nucl. Instrum. Methods A **479** (2002) 117. doi:10.1016/S0168-9002(01)02013-7.

[10] LeptonID group and Belle II Collaboration, Muon and electron identification efficiencies and hadron-lepton misidentification rates at Belle II for Moriond 2021, Mar 2021. BELLE2-CONF-PH-2021-002.

[11] Kuraray, Ltd. (Japan), https://www.kuraray.com/products/psf[Accessed 25 Feb 2024]

[12] T. Aushev, D. Z. Besson, K. Chilikin *et al.*, A scintillator based endcap K and muon detector for the Belle II experiment. Nucl. Instrum. Methods A **789** (2015) 134 doi:10.1016/j.nima.2015.03.060

[13] X. Y. Wang, H. Y. Zhang, D. Q. Fang *et al.*, Design and performance of a high-speed and low-noise preamplifier for SiPM. Nucl. Sci. Tech. **34** (2023) 169 doi:10.1007/s41365-023-01328-7

[14] BEIJING GAONENG KEDI TECHNOLOGY CO. Ltd. (China), http://www.gaonengkedi.com/[Accessed 25 Feb 2024]

[15] A. Pla-Dalmau, A. D. Bross and K. L. Mellott, Low-cost extruded plastic scintillator. Nucl. Instrum. Methods A **466** (2001) 482 doi: 10.1016/S0168-9002(01)00177-2.

[16] Saint-Gobain, Ltd. (France), https://luxiumsolutions.com/sites/default/files/2021-11/Fiber-Product-Sheet.pdf[Accessed 25 Feb 2024]

[17] J. N. Dong, Y. L. Zhang, Z. Y. Zhang *et al.*, Position-sensitive plastic scintillator detector with WLS-fiber readout. Nucl. Sci. Tech. **29** (2018) 117. doi:10.1007/s41365-018-0449-2.

[18] K. Wang, S. Samaranayake and A. Estrade, Investigation of a digitizer for the plastic scintillation detectors of time-of-flight mass measurements. Nucl. Instrum. Methods A **1027** (2022) 166050. doi:10.1016/j.nima.2021.166050.